

Thermally Strain-Induced Band Gap Opening on Platinum Diselenide-Layered Films: A Promising Two-Dimensional Material with Excellent Thermoelectric Performance

Teng-Yu Su,^{††} Te-Hsien Wang,^{††} Deniz P. Wong, Yi-Chung Wang, Angus Huang, Ying-Chun Sheng, Shin-Yi Tang, Tsu-Chin Chou, Ta-Lei Chou, Horng-Tay Jeng,* Li-Chyong Chen, Kuei-Hsien Chen, and Yu-Lun Chueh*



Cite This: *Chem. Mater.* 2021, 33, 3490–3498



Read Online

ACCESS |



Metrics & More

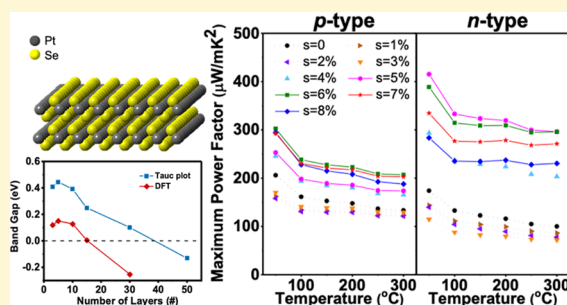


Article Recommendations



Supporting Information

ABSTRACT: In this work, we, for the first time, observed the remarkable thermoelectric properties of a few high-quality PtSe₂ layered films fabricated by a post selenization of Pt thin films. An excellent power factor of $\geq 200 \mu\text{W}/\text{mK}^2$ with a Seebeck coefficient of $>100 \mu\text{V}/\text{K}$ in the PtSe₂ layered film of 10 layers can be experimentally demonstrated over a wide temperature range, which is much better than those of most of the two-dimensional materials reported in the literature. Optical absorption spectra and DFT (density functional theory) calculations indicate a semiconductor–metal transition at a critical thickness once the thickness increases from 7.7 (15 layers) to 14.3 nm (30 Layers). The results are consistent with the experimental results of the dramatic reduction in the power factor, the magnitude of the Seebeck coefficient, and the resistivity when the thickness increases from 7.7 (15 layers) to 14.3 nm (30 Layers). Nevertheless, the semiconductor–metal transition would occur when the thickness increases from 1.5 nm (3 layers) to 2 nm (4 layers). To figure out this unusual performance, a detailed material examination has been conducted. After the transmission electron microscopy examination, $\sim 7\%$ biaxial compressive strain built in the polycrystalline PtSe₂ thin film can be observed. The strain, as revealed by our DFT calculations, plays an important role in opening the electronic energy gap and hence significantly improves the thermoelectric performance. Boltzmann transport calculation results suggested that both the strain and the hole concentration in the p-type specimens are well optimized. We further propose that an even better power factor can be achieved with n-type doped PtSe₂.



1. INTRODUCTION

Thermoelectric power generators, which can directly harvest electrical energy from a temperature gradient, have attracted great attention in resolving the escalating energy crisis.^{1–5} The thermoelectric efficiency governed by the figure of merit, $zT = S^2\sigma T/\kappa$, is used to reflect the efficiency of thermal energy conversion where S , σ , κ , and T represent the Seebeck coefficient, electrical conductivity, thermal conductivity, and absolute temperature, respectively. Among various available materials for thermoelectric applications, two dimensional (2D) layered semiconductors, especially transition metal dichalcogenides (TMDCs), have been attracted intensive attention because of their special properties and potential for electronics.^{6–8}

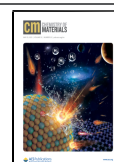
TMDCs are layered structures with transition metals (i.e., Mo, W, and Ta) at the center sandwiched by two chalcogen atoms (S, Se, and Te). Owing to the various combinations of transition metals and chalcogens, they exhibit diverse properties, promising for versatile applications.^{9,10} For example, the indirect-to-direct band gap transition in MoS₂ from the bulk to

monolayer opens the ways to its applications in optoelectronics.^{11,12} Several groups also have demonstrated that some TMDCs, such as MoS₂¹³ and WS₂,¹⁰ have a large magnitude of the Seebeck coefficient. However, their low electrical conductivity deteriorates their thermoelectric performance, which makes them being incompatible with common thermoelectric materials, such as Bi₂Te₃¹⁴ and Sb₂Te₃.¹⁵ Although the reported thermoelectric results of some TMDCs are not good, the TMDCs with a tunable bandgap and a high mobility such as PtSe₂ would be promising candidates as excellent thermoelectric materials.⁴⁴ The electronic structure of the PtSe₂ layered film is highly sensitive to its thickness. An unstrained single-crystalline monolayer PtSe₂ is a semiconductor with a

Received: November 11, 2020

Revised: February 12, 2021

Published: May 5, 2021



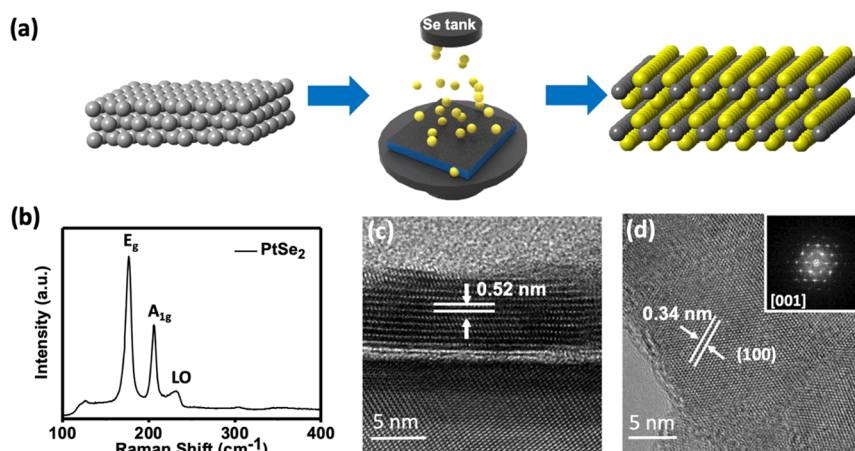


Figure 1. (a) Schematic process for fabrication of PtSe₂ layered films. (b) Characteristic Raman spectrum of the PtSe₂ layered film. (c,d) Cross-sectional and top view TEM images of the PtSe₂ layered film.

band gap up to 1.3 eV, and it becomes metallic when its thickness increases to three layers.^{16,17}

Moreover, it has been reported that the PtSe₂ layered film is suggested as a good thermoelectric material because of its pudding-mold type electronic structure, consisting of a dispersive and flat portion, which is beneficial to the coexistence of a large magnitude Seebeck coefficient and high electrical conductivity.^{18,19} In addition, the electronic structure of the PtSe₂ layered films is sensitive to not only the thickness but also the strain.^{20,21} It has been predicted that the biaxial strain can significantly enhance the thermoelectric performance of the monolayer PtSe₂ layered films with both n-type and p-type doping treatments. Although the previous calculation results suggested that the PtSe₂ layered film would be a good thermoelectric material, no experimental demonstration of the thermoelectric performance of the PtSe₂ layered films has been reported yet. PtSe₂ can be fabricated by two kinds of methods, one is the top-down method, which is mechanical exfoliation,^{43,44} the other is the bottom-up method, including chemical vapor deposition (CVD)^{22,23} and post-selenization.^{24,41} Fabrication of PtSe₂ with a single domain and less defects using the top-down method can be the best method. However, the size of PtSe₂ is small, which is not suitable for mass production. On the other hand, the CVD process can also provide high-quality PtSe₂ layered thin films with a single domain but a small size.

In this regard, we fabricated PtSe₂ layered films using the selenization process on Pt thin films, which provided a larger area with a patternable process for mass production. Moreover, the PtSe₂ thin film exhibits a great thermoelectric performance with a good thermoelectric power factor, a large magnitude of the Seebeck coefficient, and low resistivity in the specimens of thickness ≤ 7.7 nm (15 layers). The results also reveal a semiconductor-to-metal transition with a critical thickness larger than 7.7 nm (15 layers), which is much larger than those reported previously,^{16,17} while they are in agreement with optical absorption measurements and calculations of density functional theory (DFT). To investigate the outstanding thermoelectric performance of the PtSe₂ layered films with a thickness > 3 layers, detailed material characterization was conducted. Here, we mainly focus on the PtSe₂ layered film with 10 layers, which shows the best power factor of ~ 245 $\mu\text{W}/\text{mK}^2$ that is much larger than those of most of the 2D materials.^{10,13,25–33} In addition, a biaxial compressive strain of

$\sim 7\%$ built in the PtSe₂ layered film was confirmed by the fast Fourier transform analysis of the transmission electron microscopy (TEM) image and it may open the electronic gap, yielding an increase in the critical thickness of semiconductor-to-metal transition as revealed using the DFT calculations. Both the Seebeck coefficient and the Hall coefficient exhibit positive values, suggesting the hole doping in the PtSe₂ layered films, which are consistent with the p-type transistor behaviors.³⁴ With the help of DFT calculations, we found that both the hole concentration and strain in the PtSe₂ layered film with 10 layers are nearly optimized. To realize high-efficiency thermoelectric devices, both p-type- and n-type-doped PtSe₂ layered films are necessary and they can be synthesized through a controllable selenization process³⁵ or other methods.^{23,36,44} Based on the DFT calculations, the n-type doping of the PtSe₂ layered films is expected to show a better thermoelectric performance because of the multiple valleys near the conduction-band minimum (CBM), providing a new route to high-efficiency thermoelectric devices based on 2D materials.

2. RESULTS AND DISCUSSION

The PtSe₂ layered films were fabricated by the postselenization process at 600 °C with a Pt thin film prepared by the sputtering process as schematically shown in Figure 1a. The detailed experimental processes are mentioned in the experimental section. Here, the Pt thin films with thicknesses ranging from 2 to 25 nm were deposited on the sapphire substrates. Subsequently, the samples were placed in our home-made vertical furnace system to proceed selenization process to form the PtSe₂ layered films with different numbers of layers precisely. To confirm the quality of the PtSe₂ layered films, the Raman results of the PtSe₂ layered films with the 2.5 nm in thickness were measured as shown in Figure 1b. There are three peaks, among which, two strong peaks at 175 and 205 cm^{-1} can be assigned to E_g and A_{1g} phonon modes, respectively. The broad peak at ~ 230 cm^{-1} can be related to the overlap of A_{2u} and E_u longitudinal optical (LO) modes, involving the out-of-plane and in-plane motions of Pt and Se atoms.^{34,42} To further investigate the microstructure of the PtSe₂ layered film, TEM observation was conducted. The cross-sectional and plan-view images of the PtSe₂ layered film are shown in Figure 1c,d, respectively. Clearly, a layered structure with an interlayer distance of ~ 0.52 nm along the

(0001) facet can be confirmed as shown in Figure 1c. Furthermore, even the thickness of the Pt thin film reaches ~ 25 nm, and complete PtSe₂ multilayers (~ 50 layers) can be found after the selenization process as shown in Figure S1. By further elemental mapping with energy-dispersive system (EDS) analysis, we found that Pt and Se signals distribute uniformly without gradient (Figure S2), confirming that the Pt film is fully transformed into the PtSe₂ layered film. Unlike the previous study that the unreacted Pt was observed in the monolayer PtSe₂ formed by the postselenization process with the single crystalline Pt thin film.¹⁶ The Pt precursor of the current work is polycrystalline and the grain boundary can accelerate the diffusion of Se atoms into the Pt thin film to completely form the PtSe₂ phase with the selenization process.¹⁶ To observe the plane-view polycrystalline structure of the PtSe₂ layered film, a transfer process of the PtSe₂ layered film on the Cu grid by a conventional transfer process was used as shown in Figure 1d where the domain size of approximately a few nanometers can be found (Figure S3). The formation of these small domains may be contributed by the polycrystalline structure of the Pt thin film prepared by the sputtering process.³⁷ Moreover, by fast Fourier transform, we can obtain the clear lattice constant based on the certain plane. An internal spacing of 0.35 nm along the [100] direction can be found in Figure 1d, the spacing is relatively smaller than those of the theoretical calculations (0.375 nm)³⁸ and other reports^{23,44} (0.37 nm). Furthermore, the strain can be calculated using $(\varepsilon - \varepsilon_0)/\varepsilon_0$, with which ε and ε_0 are calculated to be 0.35 and 0.375 nm, yielding the $\sim 7\%$ biaxial compressive strain existing within the PtSe₂ layered film. Such a strain difference may significantly affect the electronic structure to further influence the thermoelectric properties, which will be discussed later.

To further investigate the chemical compositions of the PtSe₂ layered film, X-ray photoelectron spectroscopy was conducted. The resulting Pt 4f and Se 3d spectra are shown in Figure 2a,b, respectively. In Figure 2a, there are two prominent peaks located at 73.8 and 77.1 eV, which are related to Pt(IV)4f_{7/2} and Pt(IV)4f_{5/2}, respectively.^{24,34} Note that no

other peaks appearing within the spectrum confirms the complete reaction between Pt and Se without the unreacted Pt(0) and/or partial selenized Pt(II) signal. For the Se 3d spectrum as shown in Figure 2b, a prominent peak was observed, which can be deconvoluted into two peaks at 55.2 and 54.4 eV, corresponding to Se(II)3d^{5/2} and Se(II)3d^{3/2}, respectively.^{24,34} No other peaks related to Se(0) can be observed, indicating the absence of the excess or unreacted Se deposition on the specimen. The thickness effect, which will be discussed later, can lead to a semiconductor-to-metal transition, and hence it is crucial to the thermoelectric properties. To investigate the thickness effect, we fabricated PtSe₂ layered films with different thicknesses from ~ 2.5 (3 layers) to ~ 25.5 nm (50 layers). Figure 2c shows the Raman spectra of the PtSe₂ layered films with different thicknesses. Distinctly, the E_g peak shifts slightly to the lower frequency region because of the stacking-induced structure change and long-range Coulombic interaction with respect to other TMDCs as the thickness increases.³⁹ The ratios of E_g/A_{1g} and LO peaks show a considerable reduction in the intensity as the thickness increases, which is the same as that reported in other studies.^{40,41} For the thickness of the PtSe₂ layered film $\geq \sim 7.7$ nm (~ 10 layers), the LO peak is nearly absent, which is in agreement with the Raman results of the commercially available bulk PtSe₂ grown by the chemical vapor transport, further confirming the high quality of the PtSe₂ layered films.⁴¹ Figure 2d shows the thickness dependence of the electronic gap determined using the optical absorption spectra and that using the DFT calculations (See Figures S4, S5, and Section 4 in Supporting Information for details). As a result, the experimental band gap is consistent with calculated band gaps, both of slightly increase when the thickness increases from ~ 2.5 nm (~ 3 layers) to ~ 3.5 nm (~ 5 layers) and then decrease when the thickness further increases, leading to the semiconductor-to-metal transition. It is worth mentioning that the band gaps of the PtSe₂ layered films in our case do not monotonically decrease but slightly increase and then decrease while the thickness increases. This unusual property can be explained by the shift of the CBM and the valence-band maximum (VBM). However, the main reasons or factors, which result in this property, are still required for further discussion. On the other hand, the band gap determined using the optical absorption may be slightly overestimated while that using the DFT calculations slightly underestimated (Supporting Information Section 4). As a result, the electronic band gap of our PtSe₂ layered films should be in between those calculated using optical absorption measurements and DFT calculations.

Figure 3a–c shows the temperature dependence of thermoelectric properties of the PtSe₂ layered films with thicknesses ranging from ~ 5 to ~ 25.5 nm (~ 10 to ~ 50 layers) measured using the commercial equipment ZEM 3, for which the schematic structure is shown in Figure S6. Note that the thickness of the PtSe₂ layered films $< \sim 5$ nm (~ 10 layers) cannot be taken into account because the resistivity is too large to be measured. The results of the positive Seebeck coefficient (Figure 3b) and the Hall coefficient (Figure 4f) reveal that all PtSe₂ layered films with a thickness > 5 nm (10 layers) show a p-type semiconducting behavior. As shown in Figure 3c, the PtSe₂ layered film with 10 layers shows an excellent power factor of $\geq 200 \mu\text{W}/\text{mK}^2$ over a wide temperature range from 50–300 °C. Because of the moderate decrease in the resistivity as well as the slight increase in the magnitude of the Seebeck

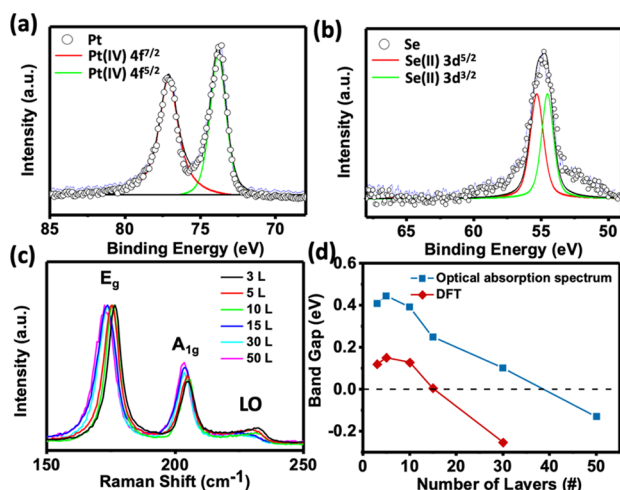


Figure 2. (a,b) Pt 4f and Se 3d XPS results of the PtSe₂ layered film. (c) Thickness dependence of the Raman spectra. (d) Thickness dependence of the electronic gap determined by the optical absorption spectra with the help of the Tauc plot and that by the DFT calculations (see Supporting Information Section 3 for details).

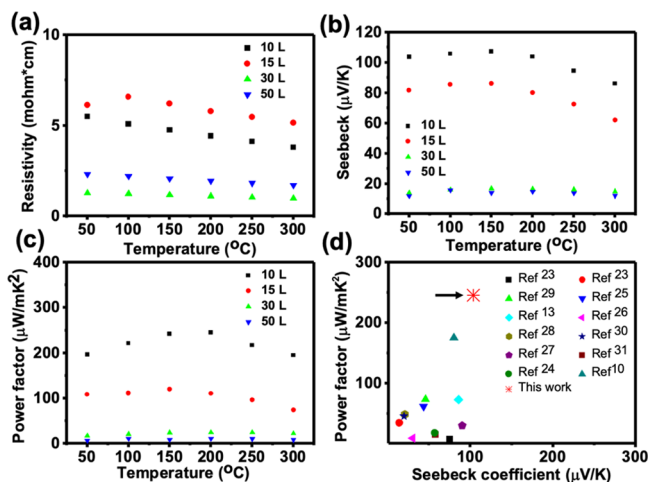


Figure 3. (a) Resistivity, (b) Seebeck coefficient, and (c) power factor of the PtSe₂ layered films with different thicknesses and temperatures ranging from 50 to 300 °C. (d) Comparison of thermoelectric performance between the 10 L PtSe₂ (present work) and other 2D materials.

coefficient (below 150 °C), the power factor increases as the temperature increases (below 200 °C). However, as the temperature further increases, the power factor decreases because of the reduction in the Seebeck coefficient regardless of the reduction of the resistivity. In contrast to the mild temperature dependence of the thermoelectric properties, the thickness dependence can be very strong. The PtSe₂ layered films with a thickness ≤ 7.7 nm (~ 15 layers) have power factors much larger than those with a thickness ≥ 14.3 nm (~ 30 layers). Interestingly, the power factor of 5 nm-thick PtSe₂ layered films (~ 10 layers) is 20 times larger than that of ~ 25.5 nm-thick (~ 50 layers) PtSe₂ layered films. Such a much larger power factor in the thinner PtSe₂ layered film is attributed to its extremely larger Seebeck coefficient even though its resistivity is also slightly higher. The dramatic reduction in both the magnitude of the Seebeck coefficient and

the resistivity with an increase in the thickness is because of the semiconductor-to-metal transition at the thicknesses between ~ 7.7 (~ 15 layers) and ~ 14.3 nm (~ 30 layers), which is in agreement with our previous results on the electronic bandgap determined using optical absorption measurements and DFT calculations and is consistent with the previous reports.^{16,17,42,43} To ensure the contribution of the good thermoelectric performance and thermal stability of the 5 nm-thick PtSe₂ layered film (10 layers), the in situ X-ray diffraction (XRD) was carried out from room temperature to 300 °C as shown in Figure S7. Distinctly, there is no degradation over all the measured temperatures in a characteristic peak located at 16.7° corresponding to the (001) plane of the PtSe₂ layered films, confirming the high thermal stability. On the other hand, aging is also an important factor to determine the quality of thermoelectric material. We measured the same sample starting from the as-fabricated conditions to the aging time of 6 months as shown in Figure S8. The power factor can be maintained almost the same value even after the aging time of 6 months, confirming the high stability of the PtSe₂ layered films. Figure 3d lists the best thermoelectric performance of the PtSe₂ layered films (10 layers) with other 2D materials and the overall results are shown in Table 1.^{10,13,25–33} Clearly, a large power factor of $245 \mu\text{W}/\text{mK}^2$ and the excellent magnitude of the Seebeck coefficient of $104 \mu\text{V}/\text{K}$ are the best thermoelectric performance compared with those of many pure 2D materials and other 2D materials assisted by the extra thermoelectric enhancement through the functionalization with metallic nanoparticles, such as Au³¹ and Ag²⁹ or hybridization with highly conductive materials, such as rGO,^{26,33} CNTs,²⁷ and PEDOT/PSS.^{30,32} It is believed that the thermoelectric performances of our PtSe₂ can be further enhanced after adding the extra thermoelectric enhancers such as functionalized metallic nanoparticles or hybridized conductive materials on the PtSe₂ layered films.

Comprehensive theoretical calculations were carried out to discover the excellent thermoelectric performance while the thickness of the PtSe₂ layered film was fixed at ~ 5 nm (~ 10 layers). Figure 4a shows the corresponding electronic structure

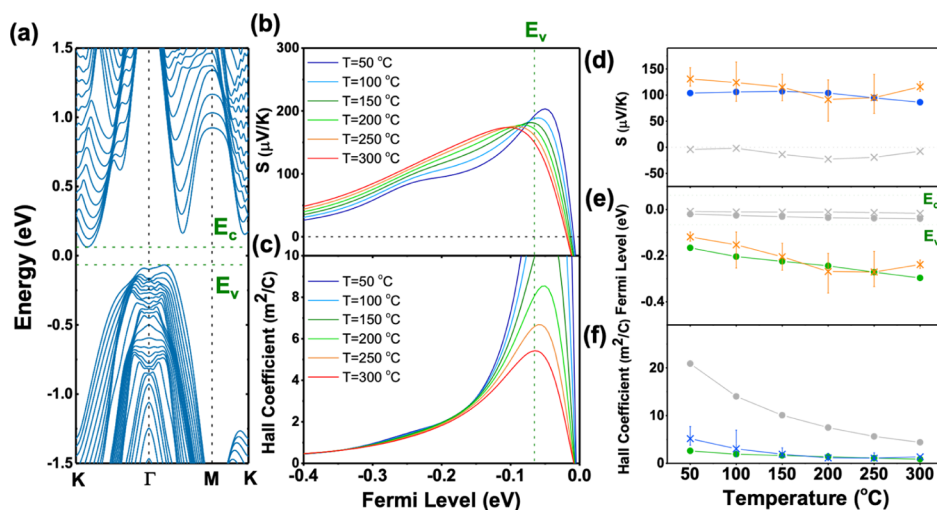


Figure 4. Electronic structure and thermoelectric properties of the PtSe₂ layered film with 10 layers under the biaxial compressive strain of 7.13%. (a) Electronic structure, (b) Seebeck coefficient, and (c) Hall coefficient as a function of Fermi level at temperatures in the range of 50–300 °C. Comparing the experimental Seebeck coefficient (Hall coefficient) indicated by the blue dot in (d) (blue cross in (f)) and the calculated results in (b,c), we can obtain two possible Fermi levels indicated by the green and gray dots (orange and gray crosses) in (e) leading to two possible values of the Hall coefficient shown in (f) (the Seebeck coefficient shown in (d)).

Table 1. Comparison of Thermoelectric Performance between the 10 L PtSe₂ (Present Work) and Other 2D Materials

material	Seebeck coefficient ($\mu\text{V}/\text{K}$)	thermoelectric power factor ($\mu\text{W}/\text{m}\cdot\text{K}^2$)	ref
WS ₂ nanobelt	75	7	25
NbSe ₂ nanobelt	14	34	25
BP with Au NP	45.6	73.4	31
1T WS ₂ with SWCNT	43.2	61.7	27
1T/2H MoS ₂	85.6	73.1	13
1T WS ₂	30	9.4	28
MoSe ₂ with PEDOT/PSS	20.6	48.6	30
MoS ₂ with PEDOT/PSS	19.5	45.6	32
MoS ₂ with Ag NP	90	30	29
MoS ₂ with rGO	58	15.1	33
WS ₂ with rGO	57	17.4	26
WS ₂ with SWCNT	80	175	10
PtSe ₂	103.9	245.1	this work

of the PtSe₂ layered films with a lattice constant of $a = 0.35$ nm obtained from the TEM results as mentioned previously. Such a lattice constant is equivalent to a biaxial compressive strain of 7.13%, leading to the metal-to-semiconductor transition with a large gap of 127 meV. Furthermore, the Hall coefficient and Seebeck coefficient, as shown in Figure 4b,c, exhibit typical semiconductor behaviors. For the p-type PtSe₂ layered film with the Fermi level below the VBM, the magnitude of the Seebeck coefficient and Hall coefficient increases with an increase in the Fermi level because of the decrease in the

carrier concentration. The magnitude of the Seebeck coefficient increases as the temperature increases, while the Hall coefficient is weakly dependent on temperature. When the Fermi level further moves toward the energy gap, both the magnitude of the Seebeck coefficient and the Hall coefficient decrease because of the bipolar effect, which becomes more severe as the temperature increases. As shown in Figure 4d, the measured Seebeck coefficient (blue dot) is up to about 100 $\mu\text{V}/\text{K}$ because of the strain-induced gap. By systematically comparing the experimental data of the Seebeck coefficient (blue line in Figure 4d) and Hall coefficient (blue line in Figure 4f) with the calculated results, we found that the Fermi level is well below the VBM (green/orange line in Figure 4e), indicating that our PtSe₂ layered films are degenerate p-type semiconductors (see Supporting Information Section 9 for details). The hole concentration might come from SeO₂ generated during the cooling process.³⁵

Figure 5a shows the temperature dependence of the maximum power factor of PtSe₂ with a 10 layer thickness under different amounts of strain. The Seebeck coefficient and the electrical conductivity can be obtained by tuning the Fermi level in the p-type PtSe₂ layered film, for which 10 layers under the biaxial compressive strain in the range of zero to 8% were used (Figures S9a,b or Sd for 50 °C). The detailed thermoelectric parameters as a function of the Fermi level for each strain are shown in Figures S10 and S11. Clearly, the power factor generally decreases with the increase in temperature because of the decrease in the electrical conductivity (Figure 5c) regardless of the increase in the magnitude of the Seebeck coefficient (Figure 5b). The reduction of the electrical conductivity as well as the relaxation time (Figure S9e) as the temperature increases indicates that the electron–phonon scattering may be the dominant scattering mechanism. Because of the critical strain triggering

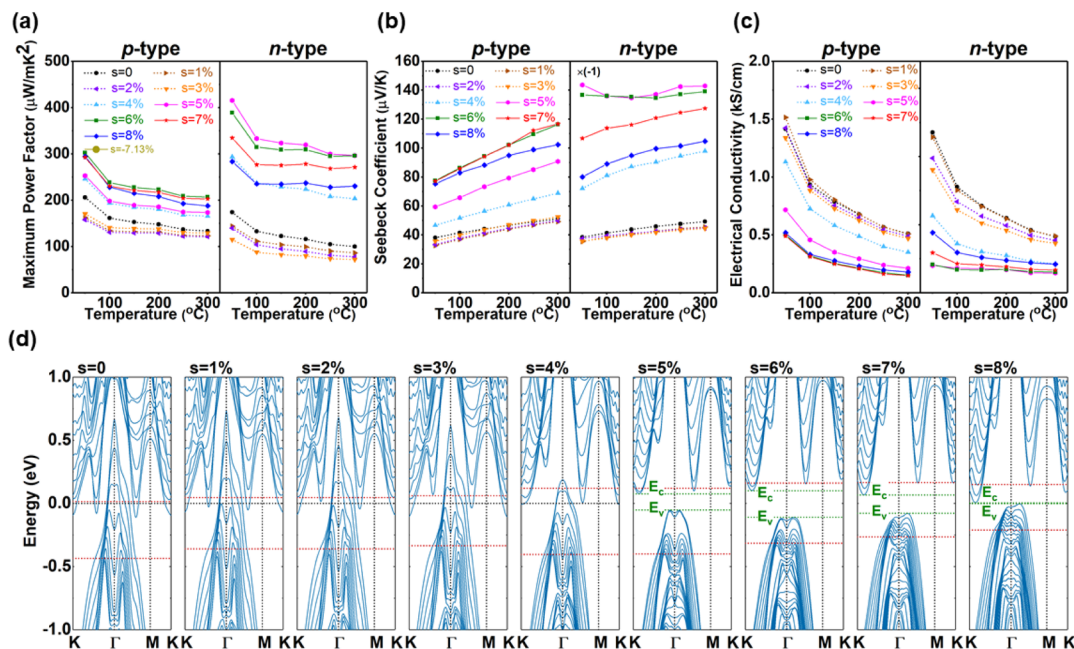


Figure 5. Thermoelectric properties as a function of temperature and electronic structures of the PtSe₂ layered film with 10 layers under biaxial compressive strains in the range of 0–8%. (a) Maximum power factors at the optimum Fermi level for both *p*-type and *n*-type systems and their corresponding (b) Seebeck coefficients and (c) electrical conductivities. (d) Evolution of the band structure with the biaxial compressive strain. Note that the energy zero is set at the intrinsic Fermi level at zero temperature, and the red line below (above) the energy zero is the optimum Fermi level for the *p*- (*n*-) type system at 50 °C. The temperature dependence of the optimum Fermi level is weak and can be seen in Figure S8a,b.

the metal-to-semiconductor transition is in the strain range of 4–5% as shown in Figure 5d, the power factor and the magnitude of the Seebeck coefficient (the electrical conductivity) under high strains of $\geq 5\%$ are generally larger (smaller) than those under a low strain of $\leq 4\%$. For p-type doping, the power factor and the magnitude of the Seebeck coefficient under a strain of 5% are significantly smaller than those of higher strains, namely 6–8%. This is because that with the strain of 5%, the highest doubly degenerate valence bands are considerably separated from the other valence bands around the Γ point, leading to an optimum Fermi level over 0.3 eV below the VBM so that the PtSe₂ layered film becomes more metallic-like with a weakened asymmetry of the electronic density of states around the Fermi level. For a higher strain of ~ 6 –8%, the highest doubly degenerate valence bands become much closer to the other valence bands, enhancing the asymmetry of the electronic density of states and hence enhancing the Seebeck coefficient and the power factor. Fortuitously, our as-grown PtSe₂ layered films with an intrinsic compressive strain of $\sim 7\%$ turn out to be already well optimized for high thermoelectric performance. In addition, the Fermi level of the PtSe₂ layered films in the range of -235 ± 65 meV, that is, ~ 0.17 eV below the VBM (Figure 4e), is close to the optimum Fermi level within -245 ± 10 meV, that is, ~ 0.18 eV below the VBM (Figure S9a). Re-enforced by these two factors, our measured power factor is as high as 200 W/mK^2 (Figure 3c), being in good agreement with the calculated maximum power factor as shown in Figure 5a. To achieve high-efficiency thermoelectric devices, an n-type material of a large power factor is also indispensable. Therefore, the optimized thermoelectric properties of the n-type PtSe₂ layered film are also included in Figure 5a–c. Clearly, our predicted maximum power factor for the n-type PtSe₂ film is even higher than that of the p-type-doped film of $\sim 100 \text{ W/mK}^2$. Such a high power factor for the n-type PtSe₂ film with 10 layers is mainly because of the multivalley effect, which was observed in many good thermoelectric materials such as Bi₂Te₃,⁴⁴ PbTe,⁴⁵ SnSe,⁴⁶ and CoSb₃.⁴⁷ For the strain of 5%, the second (third) lowest CBM along the ΓM (MK) is only 19 (61) meV higher than the lowest CBM, leading to the highest power factor as shown in Figure 5a. When the strain further increases, the energy difference between the second (third) and the lowest CBMs increases, resulting in a decrease in the power factor. Nevertheless, the maximum power factor of n-type doping is still much larger than p-type doping for the strain not larger than 7%. In addition to the power factor, the thermal conductivity is also an important property that determines a good thermoelectric material. However, we carried out theoretical calculations to predict the performance of PtSe₂ and the detail results (Supporting Information 10). According to our simulation and experimental results, the ZT value of our PtSe₂ is between 0.02 and 0.1 for different average grain sizes. Although the value is not as good as those of traditional thermoelectric materials, such as Bi₂Te₃ and SnSe, the PtSe₂ layered film still shows a high zT value than that of the TMDC hybrid material, WS₂/rGO ($zT = 6.8 \times 10^{-4}$).²⁶ We believe that the thermoelectric property of PtSe₂ layered film can be further enhanced by utilizing similar approaches.

3. CONCLUSIONS

In summary, we fabricated high-quality PtSe₂ layered films using the postselenization process with the sputtered Pt thin films. Through comprehensive material analyses, the chemical

bonding and the crystal structure of the PtSe₂ layered films were investigated. The X-ray photoelectron spectroscopy (XPS) results ensure the complete selenization without other compounds such as Pt_xSe_{2(1-x)} or unreacted Pt metal films. The TEM results reveal a nearly 7% biaxial compressive strain built in the polycrystalline PtSe₂ layered films. Our theoretical calculations show that the biaxial compressive strain can assist to open the band gap, leading to a large magnitude of the Seebeck coefficient. The measured thermoelectric properties of the 5 nm-thick (10 layers) PtSe₂ layered film are much better than those of most of the 2D materials with high thermal stability. The thermoelectric power factor is better than 200 W/mK^2 with the Seebeck coefficient higher than 100 W/K over a wide temperature range above room temperature. In addition, the power factor, Seebeck coefficient, and resistivity dramatically decrease when the film thickness increases from 7.7 nm (15 layers) to 14.3 nm (30 layers), indicating a semiconductor-to-metal transition in agreement with our results of optical absorption measurements and DFT electronic bands. Based on the Boltzmann transport investigations, both the strain and hole concentrations of the p-type PtSe₂ layered film are well optimized, leading to the nearly highest power factor. Moreover, the n-type PtSe₂ layered film, mainly because of its multivalley effect, is predicted to have an even better power factor ($>300 \text{ W/mK}^2$) over a wide temperature range above room temperature. The outstanding thermoelectric performance above room temperature of the PtSe₂ thin films demonstrated in this work opens a route to realize high-efficiency power generators based on 2D materials.

4. EXPERIMENTAL SECTION

4.1. Pt Thin Film Preparation. The Pt thin film was prepared by the sputtering process, for which a Pt metal target was used the target source in an Ar atmosphere. Before the deposition of the Pt film, the chamber was pumped down to 5×10^{-6} torr to avoid contamination. During the deposition process, the chamber pressure was kept at 5 mTorr and purged with Ar as a carrier gas to react with the Pt target.

4.2. Formation of the PtSe₂ Layered Films. The PtSe₂ layered films were fabricated through a vertical furnace system equipped with two individual heating tanks. One is for heating the Se powder source and the other is used for heating the substrate. Before the fabrication process, the chamber was pumped below 1×10^{-3} torr to prevent pollution. During the synthesis process, the chamber was purged with a H₂/N₂ mixed gas with a ratio of 2:1. The Se tank was kept at 300 °C to achieve stable Se vapors and the temperature for heating the substrate was kept at 600 °C.

4.3. Measurements and Materials Characterization. Raman spectroscopy was carried out through LABRAM HR 800 UV equipped with red laser (635 nm) excitation. The microstructure was observed using a spherical-aberration corrected field emission transmission electron microscopy (Cs-corrected field emission TEM, JEOL, JEM-ARM200FTH) with an image resolution of 0.19 nm equipped with a scanning transmission electron microscope and an energy-dispersive spectrometer. The chemical bonding information was characterized by X-ray photoelectron spectroscopy PHI 5000 Versaprobe II. The optical absorption spectra were measured using an ultraviolet–visible–near-infrared spectrophotometer (Hitachi U4100) with standard mirror optics and an integrating sphere. The electrical conductivity, Seebeck coefficient, and thermoelectric power factor were measured and calculated using a commercial apparatus (ZEM-3, ULVAC-RIKO, Japan) under a helium atmosphere with a home-made holder for thin film measurements. The Hall coefficient was obtained using an in situ Hall measurement system (HMS-3000, Ecopia using the van der Pauw configuration). The Hall measurements were carried out under vacuum with a heating rate of 5 °C/minute and cooling in a vacuum. The crystalline structure was

measured using an in situ X-ray diffractometer (Shimadzu 6000) equipped with a vacuum heating stage by using Cu K α ($\lambda = 0.154$ nm) as a radiation source. The in situ XRD results were performed in a vacuum pressure of 10^{-3} Torr with a heating rate of 20 °C/min and cooling in air.

4.4. DFT Calculations. The electronic structure was calculated through the projector augmented wave (PAW) approach within the framework of DFT as implemented in the Vienna Ab initio Simulation Package (VASP).^{48–50} The exchange–correlation is described in the Perdew–Burke–Ernzerhof (PBE) form of generalized gradient approximation (GGA).^{51,52} The spin–orbit coupling was taken into account. The $12 \times 12 \times 1$ Monkhorst–Pack mesh was used for k -point sampling within the Brillouin zone. The cut-off energy for plane wave basis was set as 400 eV. The energy convergence threshold was set to 10^{-9} eV in the self-consistent calculations. The electronic dispersion calculated in this method has been demonstrated in quantitative agreement with that observed by angle-resolved photoemission spectroscopy for PtSe₂.⁵³ For structure relaxation, the van der Waals interactions between two adjacent PtSe₂ layered films were included using the DFT-D3 method with Becke–Johnson damping.^{54,55} All the internal atomic coordinates are relaxed until the magnitude of the force acting on all atoms is less than 0.002 eV/Å. For the unstrained case, the lattice constant is also relaxed, leading to a lattice constant of $a = 0.377$ nm.^{53,56,57} The electrical conductivity, Seebeck coefficient, and Hall coefficient were calculated through the Boltzmann transport equation with the relaxation time approximation, which can be found in refs 58 and 59. The temperature dependence of the relaxation time (Figure S9e) is obtained by fitting the experimental resistivity (Figure 3a) of the p -type 10 L PtSe₂ under the biaxial compressive strain $s = 7.13\%$ to the solution of the Boltzmann transport equation with the Fermi level (blue line in Figure 4e) obtained by fitting the experimental Seebeck coefficient (blue line in Figure 4d). Here, we do not use the Fermi level obtained by fitting the measured Hall coefficient because the specimens used for the Hall measurement are different from those used for the electrical conductivity and Seebeck coefficient measurements. Even though both specimens were made from the same process, their properties may slightly vary from sample to sample. For comparison purpose as well as because of the lack of specimens with various doping levels and strains, the same relaxation times are used in all our calculations, including the cases of n -type doping and other strains. This would give rather conservative estimations of the relaxation times and hence the power factors because of the relatively high density of states of the p -type 10 L PtSe₂ under the strain of $s \sim 7\%$ as discussed in Supporting Information Section 8.

■ ASSOCIATED CONTENT

SI Supporting Information

The Supporting Information is available free of charge at <https://pubs.acs.org/doi/10.1021/acs.chemmater.0c04351>.

Detailed experimental sections; TEM image of a PtSe₂ layered film with a thickness of 25.5 nm (50 layers); EDS analysis of the PtSe₂ layered film with a thickness of 25.5 nm (50 layers); thickness dependence of the electronic gap; schematic of thermoelectric measurements; in situ XRD results of PtSe₂ layered film with a thickness of 5 nm (10 layers); thermoelectric properties as a function of Fermi level; and determination of the Fermi level position (PDF)

■ AUTHOR INFORMATION

Corresponding Authors

Horng-Tay Jeng – Department of Physics, National Tsing Hua University, Hsinchu 30013, Taiwan; Physics Division, National Center for Theoretical Sciences, Hsinchu 30013, Taiwan; Institute of Physics, Academia Sinica, Taipei 11529,

Taiwan; orcid.org/0000-0002-2881-3826; Phone: +886 3 5742515; Email: jeng@phys.nthu.edu.tw

Yu-Lun Chueh – Department of Materials Science and Engineering and Frontier Research Center on Fundamental and Applied Sciences of Matters, National Tsing Hua University, Hsinchu 30013, Taiwan; Department of Physics, National Sun Yat-Sen University, Kaohsiung 80424, Taiwan; orcid.org/0000-0002-0155-9987; Phone: +886 3 5715131 ext 33965; Email: ylchueh@mx.nthu.edu.tw

Authors

Teng-Yu Su – Department of Materials Science and Engineering and Frontier Research Center on Fundamental and Applied Sciences of Matters, National Tsing Hua University, Hsinchu 30013, Taiwan; Department of Physics, National Sun Yat-Sen University, Kaohsiung 80424, Taiwan

Te-Hsien Wang – Department of Applied Science, National Taitung University, Taitung 95092, Taiwan

Deniz P. Wong – Center for Condensed Matter Sciences, National Taiwan University, Taipei 10617, Taiwan; orcid.org/0000-0001-7126-0019

Yi-Chung Wang – Department of Materials Science and Engineering and Frontier Research Center on Fundamental and Applied Sciences of Matters, National Tsing Hua University, Hsinchu 30013, Taiwan; Department of Physics, National Sun Yat-Sen University, Kaohsiung 80424, Taiwan

Angus Huang – Department of Physics, National Tsing Hua University, Hsinchu 30013, Taiwan

Ying-Chun Sheng – Department of Materials Science and Engineering and Frontier Research Center on Fundamental and Applied Sciences of Matters, National Tsing Hua University, Hsinchu 30013, Taiwan; Department of Physics, National Sun Yat-Sen University, Kaohsiung 80424, Taiwan

Shin-Yi Tang – Department of Materials Science and Engineering and Frontier Research Center on Fundamental and Applied Sciences of Matters, National Tsing Hua University, Hsinchu 30013, Taiwan; Department of Physics, National Sun Yat-Sen University, Kaohsiung 80424, Taiwan

Tsu-Chin Chou – Institute of Analytical and Environment Sciences, National Tsing Hua University, Hsinchu 30013, Taiwan

Ta-Lei Chou – Center for Condensed Matter Sciences, National Taiwan University, Taipei 10617, Taiwan

Li-Chyong Chen – Center for Condensed Matter Sciences, National Taiwan University, Taipei 10617, Taiwan

Kuei-Hsien Chen – Center for Condensed Matter Sciences, National Taiwan University, Taipei 10617, Taiwan; Institute of Atomic and Molecular Sciences, Academia Sinica, Taipei 10617, Taiwan

Complete contact information is available at: <https://pubs.acs.org/doi/10.1021/acs.chemmater.0c04351>

Author Contributions

†† T.Y.S. and T.H.W. contributed equally to this work.

Notes

The authors declare no competing financial interest.

■ ACKNOWLEDGMENTS

This work was supported by the Ministry of Science and Technology, Taiwan. J.H.T. also thanks the CQT-NTHU, MOE, iMATE-AS, NCHC, and CINC-NTU, Taiwan for technical support. The research is supported by Ministry of

Science and Technology through grant nos., 108-2218-E-007-045-, 107-2923-E-007-002-MY3, 107-2218-E-007-055-, 107-2112-M-007 -030-MY3, 109-2634-F-007-023, 109-2221-E-007-048-, 109-2112-M-143-001-MY3, 109-2112-M-007 -034 -MY3 and 107-2628-M-110-001-MY3. Y.L. Chueh greatly appreciates the use of facility at CNMM.

REFERENCES

- (1) Bell, L. E. Cooling, Heating, Generating Power, and Recovering Waste Heat with Thermoelectric Systems. *Science* **2008**, *321*, 1457–1461.
- (2) Snyder, G. J.; Toberer, E. S. Complex thermoelectric materials. *Materials for Sustainable Energy: A Collection of Peer-Reviewed Research and Review Articles from Nature Publishing Group*; World Scientific, 2011; pp 101–110.
- (3) He, J.; Tritt, T. M. Advances in thermoelectric materials research: Looking back and moving forward. *Science* **2017**, *357*, No. eaak9997.
- (4) Zhu, T.; Liu, Y.; Fu, C.; Heremans, J. P.; Snyder, J. G.; Zhao, X. Compromise and Synergy in High-Efficiency Thermoelectric Materials. *Adv. Mater.* **2017**, *29*, 1605884.
- (5) Beretta, D.; Neophytou, N.; Hodges, J. M.; Kanatzidis, M. G.; Narducci, D.; Martin-Gonzalez, M.; Beekman, M.; Balke, B.; Cerretti, G.; Tremel, W.; Zevalkink, A.; Hofmann, A. I.; Müller, C.; Dörling, B.; Campoy-Quiles, M.; Caironi, M. Thermoelectrics: From history, a window to the future. *Mater. Sci. Eng., R* **2019**, *138*, 100501.
- (6) Geim, A. K. Graphene: Status and Prospects. *Science* **2009**, *324*, 1530–1534.
- (7) Liu, H.; Neal, A. T.; Zhu, Z.; Luo, Z.; Xu, X.; Tománek, D.; Ye, P. D. Phosphorene: An Unexplored 2D Semiconductor with a High Hole Mobility. *ACS Nano* **2014**, *8*, 4033–4041.
- (8) Ni, Z.; Liu, Q.; Tang, K.; Zheng, J.; Zhou, J.; Qin, R.; Gao, Z.; Yu, D.; Lu, J. Tunable Bandgap in Silicene and Germanene. *Nano Lett.* **2012**, *12*, 113–118.
- (9) Chhowalla, M.; Shin, H. S.; Eda, G.; Li, L.-J.; Loh, K. P.; Zhang, H. The chemistry of two-dimensional layered transition metal dichalcogenide nanosheets. *Nat. Chem.* **2013**, *5*, 263–275.
- (10) Coleman, J. N.; Lotya, M.; O'Neill, A.; Bergin, S. D.; King, P. J.; Khan, U.; Young, K.; Gaucher, A.; De, S.; Smith, R. J.; Shvets, I. V.; Arora, S. K.; Stanton, G.; Kim, H.-Y.; Lee, K.; Kim, G. T.; Duesberg, G. S.; Hallam, T.; Boland, J. J.; Wang, J. J.; Donegan, J. F.; Grunlan, J. C.; Moriarty, G.; Shmeliov, A.; Nicholls, R. J.; Perkins, J. M.; Grievson, E. M.; Theuwissen, K.; McComb, D. W.; Nellist, P. D.; Nicolosi, V. Two-Dimensional Nanosheets Produced by Liquid Exfoliation of Layered Materials. *Science* **2011**, *331*, 568–571.
- (11) Radisavljevic, B.; Radenovic, A.; Brivio, J.; Giacometti, V.; Kis, A. Single-layer MoS₂ transistors. *Nat. Nanotechnol.* **2011**, *6*, 147–150.
- (12) Yin, Z.; Li, H.; Li, H.; Jiang, L.; Shi, Y.; Sun, Y.; Lu, G.; Zhang, Q.; Chen, X.; Zhang, H. Single-Layer MoS₂ Phototransistors. *ACS Nano* **2012**, *6*, 74–80.
- (13) Huang, H.; Cui, Y.; Li, Q.; Dun, C.; Zhou, W.; Huang, W.; Chen, L.; Hewitt, C. A.; Carroll, D. L. Metallic 1T phase MoS₂ nanosheets for high-performance thermoelectric energy harvesting. *Nano Energy* **2016**, *26*, 172–179.
- (14) Venkatasubramanian, R.; Siivola, E.; Colpitts, T.; O'Quinn, B. Thin-film thermoelectric devices with high room-temperature figures of merit. *Nature* **2001**, *413*, 597.
- (15) Zhang, Y.; Snedaker, M. L.; Birkel, C. S.; Mubeen, S.; Ji, X.; Shi, Y.; Liu, D.; Liu, X.; Moskovits, M.; Stucky, G. D. Silver-Based Intermetallic Heterostructures in Sb₂Te₃ Thick Films with Enhanced Thermoelectric Power Factors. *Nano Lett.* **2012**, *12*, 1075–1080.
- (16) Wang, Y.; Li, L.; Yao, W.; Song, S.; Sun, J. T.; Pan, J.; Ren, X.; Li, C.; Okunishi, E.; Wang, Y.-Q.; Wang, E.; Shao, Y.; Zhang, Y. Y.; Yang, H.-t.; Schwiery, E. F.; Iwasawa, H.; Shimada, K.; Taniguchi, M.; Cheng, Z.; Zhou, S.; Du, S.; Pennycook, S. J.; Pantelides, S. T.; Gao, H.-J. Monolayer PtSe₂, a New Semiconducting Transition-Metal-Dichalcogenide, Epitaxially Grown by Direct Selenization of Pt. *Nano Lett.* **2015**, *15*, 4013–4018.
- (17) Kandemir, A.; Akbali, B.; Kahraman, Z.; Badalov, S. V.; Ozcan, M.; Iyikanat, F.; Sahin, H. Structural, electronic and phononic properties of PtSe₂: from monolayer to bulk. *Semicond. Sci. Technol.* **2018**, *33*, 085002.
- (18) Usui, H.; Kuroki, K.; Nakano, S.; Kudo, K.; Nohara, M. Pudding-Mold-Type Band as an Origin of the Large Seebeck Coefficient Coexisting with Metallic Conductivity in Carrier-Doped FeAs₂ and PtSe₂. *J. Electron. Mater.* **2014**, *43*, 1656–1661.
- (19) Usui, H.; Suzuki, K.; Kuroki, K.; Nakano, S.; Kudo, K.; Nohara, M. Large Seebeck effect in electron-doped FeAs₂ driven by a quasi-one-dimensional pudding-mold-type band. *Phys. Rev. B: Condens. Matter Mater. Phys.* **2013**, *88*, 075140.
- (20) Li, P.; Li, L.; Zeng, X. C. Tuning the electronic properties of monolayer and bilayer PtSe₂ via strain engineering. *J. Mater. Chem. C* **2016**, *4*, 3106–3112.
- (21) Guo, S.-D. Biaxial strain tuned thermoelectric properties in monolayer PtSe₂. *J. Mater. Chem. C* **2016**, *4*, 9366–9374.
- (22) Yu, X.; Yu, P.; Wu, D.; Singh, B.; Zeng, Q.; Lin, H.; Zhou, W.; Lin, J.; Suenaga, K.; Liu, Z.; Wang, Q. J. Atomically thin noble metal dichalcogenide: a broadband mid-infrared semiconductor. *Nat. Commun.* **2018**, *9*, 1545.
- (23) Wang, Z.; Li, Q.; Besenbacher, F.; Dong, M. Facile Synthesis of Single Crystal PtSe₂ Nanosheets for Nanoscale Electronics. *Adv. Mater.* **2016**, *28*, 10224–10229.
- (24) Chia, X.; Adriano, A.; Lazar, P.; Sofer, Z.; Luxa, J.; Pumera, M. Layered Platinum Dichalcogenides (PtS₂, PtSe₂, and PtTe₂) Electroanalysis: Monotonic Dependence on the Chalcogen Size. *Adv. Funct. Mater.* **2016**, *26*, 4306–4318.
- (25) Oh, J. Y.; Lee, J. H.; Han, S. W.; Chae, S. S.; Bae, E. J.; Kang, Y. H.; Choi, W. J.; Cho, S. Y.; Lee, J.-O.; Baik, H. K.; Lee, T. I. Chemically exfoliated transition metal dichalcogenide nanosheet-based wearable thermoelectric generators. *Energy Environ. Sci.* **2016**, *9*, 1696–1705.
- (26) Kim, S.; Bark, H.; Nam, S.; Choi, H.; Lee, H. Control of Electrical and Thermal Transport Properties by Hybridization of Two-Dimensional Tungsten Disulfide and Reduced Graphene Oxide for Thermoelectric Applications. *ACS Sustainable Chem. Eng.* **2018**, *6*, 15487–15493.
- (27) Piao, M.; Li, C.; Joo, M.-K.; Chu, J.; Wang, X.; Chi, Y.; Zhang, H.; Shi, H. Hydrothermal Synthesis of Stable 1T-WS₂ and Single-Walled Carbon Nanotube Hybrid Flexible Thin Films with Enhanced Thermoelectric Performance. *Energy Technol.* **2018**, *6*, 1921–1928.
- (28) Piao, M.; Chu, J.; Wang, X.; Chi, Y.; Zhang, H.; Li, C.; Shi, H.; Joo, M.-K. Hydrothermal synthesis of stable metallic 1T phase WS₂ nanosheets for thermoelectric application. *Nanotechnology* **2017**, *29*, 025705.
- (29) Li, X.; Wang, T.; Jiang, F.; Liu, J.; Liu, P.; Liu, G.; Xu, J.; Liu, C.; Jiang, Q. Optimizing thermoelectric performance of MoS₂ films by spontaneous noble metal nanoparticles decoration. *J. Alloys Compd.* **2019**, *781*, 744–750.
- (30) Li, X.; Liu, C.; Wang, T.; Wang, W.; Wang, X.; Jiang, Q.; Jiang, F.; Xu, J. Preparation of 2D MoSe₂/PEDOT:PSS composite and its thermoelectric properties. *Mater. Res. Express* **2017**, *4*, 116410.
- (31) An, C. J.; Kang, Y. H.; Lee, C.; Cho, S. Y. Preparation of Highly Stable Black Phosphorus by Gold Decoration for High-Performance Thermoelectric Generators. *Adv. Funct. Mater.* **2018**, *28*, 1800532.
- (32) Jiang, F.; Xiong, J.; Zhou, W.; Liu, C.; Wang, L.; Zhao, F.; Liu, H.; Xu, J. Use of organic solvent-assisted exfoliated MoS₂ for optimizing the thermoelectric performance of flexible PEDOT:PSS thin films. *J. Mater. Chem. A* **2016**, *4*, S265–S273.
- (33) Wang, T.; Liu, C.; Jiang, F.; Xu, Z.; Wang, X.; Li, X.; Li, C.; Xu, J.; Yang, X. Solution-processed two-dimensional layered heterostructure thin-film with optimized thermoelectric performance. *Phys. Chem. Chem. Phys.* **2017**, *19*, 17560–17567.
- (34) Su, T.-Y.; Medina, H.; Chen, Y.-Z.; Wang, S.-W.; Lee, S.-S.; Shih, Y.-C.; Chen, C.-W.; Kuo, H.-C.; Chuang, F.-C.; Chueh, Y.-L. Phase-Engineered PtSe₂-Layered Films by a Plasma-Assisted Selenization Process toward All PtSe₂-Based Field Effect Transistor

to Highly Sensitive, Flexible, and Wide-Spectrum Photoresponse Photodetectors. *Small* **2018**, *14*, 1800032.

(35) Xu, H.; Zhang, H.; Liu, Y.; Zhang, S.; Sun, Y.; Guo, Z.; Sheng, Y.; Wang, X.; Luo, C.; Wu, X.; Wang, J.; Hu, W.; Xu, Z.; Sun, Q.; Zhou, P.; Shi, J.; Sun, Z.; Zhang, D. W.; Bao, W. Controlled Doping of Wafer-Scale PtSe₂ Films for Device Application. *Adv. Funct. Mater.* **2019**, *29*, 1805614.

(36) Ali Umar, A.; Md Saad, S. K.; Mat Salleh, M. Scalable Mesoporous Platinum Diselenide Nanosheet Synthesis in Water. *ACS Omega* **2017**, *2*, 3325–3332.

(37) Li, X.; Zhu, Y.; Cai, W.; Borysiak, M.; Han, B.; Chen, D.; Piner, R. D.; Colombo, L.; Ruoff, R. S. Transfer of Large-Area Graphene Films for High-Performance Transparent Conductive Electrodes. *Nano Lett.* **2009**, *9*, 4359–4363.

(38) Zhang, W.; Qin, J.; Huang, Z.; Zhang, W. The mechanism of layer number and strain dependent bandgap of 2D crystal PtSe₂. *J. Appl. Phys.* **2017**, *122*, 205701.

(39) Lee, C.; Yan, H.; Brus, L. E.; Heinz, T. F.; Hone, J.; Ryu, S. Anomalous Lattice Vibrations of Single- and Few-Layer MoS₂. *ACS Nano* **2010**, *4*, 2695–2700.

(40) Yim, C.; Lee, K.; McEvoy, N.; O'Brien, M.; Riazimehr, S.; Berner, N. C.; Cullen, C. P.; Kotakoski, J.; Meyer, J. C.; Lemme, M. C.; Duesberg, G. S. High-Performance Hybrid Electronic Devices from Layered PtSe₂ Films Grown at Low Temperature. *ACS Nano* **2016**, *10*, 9550–9558.

(41) O'Brien, M.; McEvoy, N.; Motta, C.; Zheng, J. Y.; Berner, N. C.; Kotakoski, J.; Elibol, K.; Pennycook, T. J.; Meyer, J. C.; Yim, C.; Abid, M.; Hallam, T.; Donegan, J. F.; Sanvito, S.; Duesberg, G. S. Raman characterization of platinum diselenide thin films. *2D Mater.* **2016**, *3*, 021004.

(42) Ciarrocchi, A.; Avsar, A.; Ovchinnikov, D.; Kis, A. Thickness-modulated metal-to-semiconductor transformation in a transition metal dichalcogenide. *Nat. Commun.* **2018**, *9*, 919.

(43) Zhao, Y.; Qiao, J.; Yu, Z.; Yu, P.; Xu, K.; Lau, S. P.; Zhou, W.; Liu, Z.; Wang, X.; Ji, W.; Chai, Y. High-Electron-Mobility and Air-Stable 2D Layered PtSe₂FETs. *Adv. Mater.* **2017**, *29*, 1604230.

(44) Mishra, S. K.; Satpathy, S.; Jepsen, O. Electronic structure and thermoelectric properties of bismuth telluride and bismuth selenide. *J. Phys.: Condens. Matter* **1997**, *9*, 461–470.

(45) Pei, Y.; Shi, X.; LaLonde, A.; Wang, H.; Chen, L.; Snyder, G. J. Convergence of electronic bands for high performance bulk thermoelectrics. *Nature* **2011**, *473*, 66–69.

(46) Zhao, L.-D.; Tan, G.; Hao, S.; He, J.; Pei, Y.; Chi, H.; Wang, H.; Gong, S.; Xu, H.; Dravid, V. P.; Uher, C.; Snyder, G. J.; Wolverton, C.; Kanatzidis, M. G. Ultrahigh power factor and thermoelectric performance in hole-doped single-crystal SnSe. *Science* **2016**, *351*, 141–144.

(47) Tang, Y.; Gibbs, Z. M.; Agapito, L. A.; Li, G.; Kim, H.-S.; Nardelli, M. B.; Curtarolo, S.; Snyder, G. J. Convergence of multi-valley bands as the electronic origin of high thermoelectric performance in CoSb₃ skutterudites. *Nat. Mater.* **2015**, *14*, 1223–1228.

(48) Kresse, G.; Furthmüller, J. Efficiency of Ab-Initio Total Energy Calculations for Metals and Semiconductors Using a Plane-Wave Basis Set. *Comput. Mater. Sci.* **1996**, *6*, 15–50.

(49) Kresse, G. Ab initio molecular dynamics for liquid metals. *J. Non-Cryst. Solids* **1995**, *192–193*, 222–229.

(50) Kresse, G.; Furthmüller, J. Efficient Iterative Schemes for Ab Initio Total-Energy Calculations Using a Plane-Wave Basis Set. *Phys. Rev. B: Condens. Matter Mater. Phys.* **1996**, *54*, 11169–11186.

(51) Perdew, J. P.; et al. Atoms, Molecules, Solids, and Surfaces: Applications of the Generalized Gradient Approximation for Exchange and Correlation. *Phys. Rev. B: Condens. Matter Mater. Phys.* **1992**, *46*, 6671–6687.

(52) Perdew, J. P.; Wang, Y. Pair-Distribution Function and Its Coupling-Constant Average for the Spin-Polarized Electron-Gas. *Phys. Rev. B: Condens. Matter Mater. Phys.* **1992**, *46*, 12947–12954.

(53) Li, Y. W.; et al. Topological Origin of the Type-II Dirac Fermions in PtSe₂. *Phys. Rev. Mater.* **2017**, *1*, 074202.

(54) Grimme, S.; Antony, J.; Ehrlich, S.; Krieg, H. A Consistent and Accurate Ab Initio Parametrization of Density Functional Dispersion Correction (Dft-D) for the 94 Elements H-Pu. *J. Chem. Phys.* **2010**, *132*, 154104.

(55) Grimme, S.; Ehrlich, S.; Goerigk, L. Effect of the Damping Function in Dispersion Corrected Density Functional Theory. *J. Comput. Chem.* **2011**, *32*, 1456–1465.

(56) Kandemir, A.; et al. Structural, Electronic and Phononic Properties of Ptse₂: From Monolayer to Bulk. *Semicond. Sci. Technol.* **2018**, *33*, 085002.

(57) Zhao, Y.; et al. High-Electron-Mobility and Air-Stable 2d Layered Ptse₂ Fets. *Adv. Mater.* **2017**, *29*, 1604230.

(58) Wang, T.-H.; Jeng, H.-T. Strongly Enhanced Thermoelectric Performance over a Wide Temperature Range in Topological Insulator Thin Films. *ACS Appl. Energy Mater.* **2018**, *1*, 5646–5655.

(59) Komelj, M.; et al. Origin of the Hall-Coefficient Anisotropy in the Y-Al-Ni-Co Periodic Approximant to the Decagonal Phase. *Solid State Commun.* **2009**, *149*, 515–518.